Published as: *Nat Struct Mol Biol*. 2013 January ; 20(1): 99–104.

Architecture of the major component of the type III secretion system export apparatus

Patrizia Abrusci[1], **Marta Vergara–Irigaray**[1,2], **Steven Johnson**[1], **Morgan D Beeby**[3,4,6], **David Hendrixson**[5], **Pietro Roversi**[1,7], **Miriam E Friede**[1], **Janet E Deane**[1,8], **Grant J Jensen**[3,4], **Christoph M Tang**[1], and **Susan M Lea**[1,9]

[1]Sir William Dunn School of Pathology, Oxford University, Oxford, United Kingdom

[2]Centre for Molecular Microbiology and Infection, Imperial College London, London, United Kingdom

[3]Department of Biology, California Institute of Technology, Pasadena, California, USA

[4]Howard Hughes Medical Institute, California Institute of Technology, Pasadena, California, USA

[5]Department of Microbiology, UT Southwestern Medical Center, Dallas, Texas, USA

Abstract

Type III secretion systems (T3SSs) are bacterial membrane-embedded secretion nanomachines designed to export specifically targeted sets of proteins from the bacterial cytoplasm. Secretion through T3SS is governed by a subset of inner membrane proteins termed the 'export apparatus'. We show that a key member of the *Shigella flexneri* export apparatus, MxiA, assembles into a ring essential for secretion *in vivo*. The ring forming interfaces are well conserved in both non-flagellar and flagellar homologues, implying that the ring is an evolutionary conserved feature in these systems. Electron cryo-tomography reveals a T3SS-associated cytoplasmic torus of size and shape corresponding to the MxiA ring aligned to the secretion channel located between the secretion pore and the ATPase complex. This defines the molecular architecture of the dominant component of the export apparatus and allows us to propose a model for the molecular mechanisms controlling secretion.

INTRODUCTION

Type III secretion systems (T3SSs) may be broadly divided into two classes, non-flagellar or pathogenic T3SS which promote bacterial pathogenesis by secretion of effector proteins directly into host cells[1-3], and flagellar T3SS which promote bacterial motility[4]. Both types

[9]For correspondence: susan.lea@path.ox.ac.uk.
[6]Current Address: Division of Molecular Biosciences, Imperial College London, London, United Kingdom.
[7]Current Address: CIC BioGUNE, Parque Tecnológico De Bizkaia, Bilbao, Spain.
[8]Current Address: CIMR Haematology, University of Cambridge, Cambridge, United Kingdom.

Author Contributions

J.E.D., S.J. and S.M.L. initiated the project, later joined by P.A.; S.M.L. and C.M.T. supervised the project. M.E.F. and J.E.D. designed the $MxiA_C$ expression vector and did protein expression and stability trials. P.A. performed the large-scale purification, methylation, crosslinking and SPR of $MxiA_C$ and its mutants. S.J. performed the MALS experiments. P.A designed the 'Export Apparatus' co-expression vectors and purified the recombinant complex. P.A crystallized $MxiA_C$ and optimized crystals for data collection and S.M.L. soaked and handled crystals for data collection. P.A., P.R. and S.M.L. contributed to the data collection, structure determination and model building. C.M.T. and M.V.I. designed and performed the complementation and invasion assays in *S.flexneri*. D.H. created the *C. jejuni* strains and M.D.B. and G.J.J. designed and perform the Cryo-EM tomography. P.A., S.J., S.M.L. performed data analysis and wrote the manuscript. All authors read and approved the manuscript.

Accession Codes

The X-ray crystallographic data and coordinates are deposited in the Protein Data Bank with ID 4a5p

of T3SS are evolutionarily closely related, with homologues for most key flagellar T3SS components identified in the pathogenic T3SS and vice versa and with these homologous pairs showing high levels of structural conservation[4]. Thus, the overall architecture of the T3SS is generally conserved throughout speciation across both pathogenic secretion and mobility T3SS.

T3SSs span both bacterial membranes[5] with a "basal body" from which a needle or a flagellum extends. Secretion through the system is tightly regulated[6] and depends on a poorly understood set of conserved inner membrane proteins (Supplementary table 1) termed the 'export-apparatus'[7-10] aided by a cytoplasmic ATPase complex[11]. Although recent work has provided some knowledge of the order of assembly of the components of the export apparatus[7-9,12], little is known about its molecular architecture or the molecular mechanisms for control of secretion. The largest of the export apparatus proteins is a member of the FlhA superfamily; polytopic transmembrane proteins with 8 predicted trans-membrane helices followed by a large cytosolic domain. FlhA homologues have been co-localized at the base of the both flagellar and non-flagellar T3SSs[7,8], probably in multiple copies[7-9], and shown to interact with members of the FlhB superfamily[13,14], with secretion substrates in complex with their chaperones[15,16], and with the conserved ATPase and its regulators[11]. Recent atomic structures of the cytosolic domains of FlhA homologues from flagellar and pathogenic T3SSs[15,17-20] have demonstrated a conserved fold consisting of four subdomains[17,20]. However, to date, lack of structural details of the supramolecular architecture of the export apparatus has represented one of the major obstacles to deriving a mechanistic model for its activity. We therefore set out to investigate the architecture of the major component of the export apparatus in *Shigella flexneri*, MxiA.

RESULTS

$MxiA_C$ assembles into a homo-nonameric ring

We have determined the crystal structure of the ~44kDa C-terminal cytoplasmic domain of MxiA ($MxiA_C$, 318-686) (Fig. 1a, Table 1, PDB ID: 4a5p), the FlhA homologue of *Shigella flexneri*[21] a pathogen expressing the T3SS to promote colonic invasion and cell to cell spread within the host intestinal epithelium[22]. As expected, the $MxiA_C$ monomer possesses the same fold as its homologues[15,17-20] (Fig. 1b, Supplementary figure 1). Strikingly, $MxiA_C$ assembles into a nonameric ring (Fig.1a, Supplementary figure 2), making it the first T3SS protein to crystallize as a closed and planar ring, despite the fact that the biologically relevant forms of many T3SS structural proteins are assumed to be circular assemblies[23,24]. To date, in the absence of crystal structures of such rings, monomers or remodeled forms of helical arrays seen in crystals of T3SS proteins have been manipulated to model these rings to fit electron microscopy (EM) reconstructions[23,25-29]. The $MxiA_C$ nonamer (~400kDa) has an external diameter of between 110Å and 170Å and a thickness of ~55 Å, defining an inner pore of ~50Å (Fig. 1a). Although the second subdomain (SD2) has previously been noted as having a "ring forming motif"[17,20], it does not participate in forming the ring, which instead is held together primarily by interactions involving subdomains three (~60% of the ~2000$Å^2$ total interaction area per subunit) and one (~30%).

Cross-linking of the MxiA construct used for crystallization experiments ($MxiA_C$) shows that the highest oligomeric species detectable in solution has a molecular weight consistent with a nonamer (Fig. 1c). Expression of full-length MxiA as a recombinant protein in *E. coli* was challenging but co-expression of MxiA-Myc-His with the other export apparatus components (Spa24, Spa29, Spa9) has allowed us to purify an homogenous oligomer of full-length MxiA in complex with sub-stoichiometric levels of Spa24 (Supplementary figure 3). This full-length MxiA complex has an apparent molecular weight consistent with a nonamer as demonstrated by Native PAGE (Supplementary figure 3 a-c) and Multi Angle Light

Scattering MALS (Supplementary figure 3d), supporting the idea that in the bacterial membrane the native protein oligomerizes into the same multimer seen in the crystalline state.

A MxiA ring is required for T3SS secretion in vivo

To test the functional importance of the $MxiA_C$ ring we mutated residues involved in the subunit interface. In addition to the large surface area buried (~2000Å^2), the interface is stabilized by five inter-subunit salt bridges: Lys504-Asp516, Glu502-Lys548, Glu496-Arg577 and Glu532-Arg560 connect neighboring SD3s, while Arg545-Glu418 connects SD3 and SD1 (Fig. 2a, Supplementary figure 4). We therefore created a panel of mutants, including a variant called $MxiA_C$M5 abolishing all the intermolecular salt bridges (E502A, K504A, R545A, R560A and R577A). We purified the $MxiA_C$M5, which produced a circular dichroism (CD) spectrum comparable to the WT protein (Supplementary figure 5a), demonstrating that these mutations do not perturb the native folding of the protein. Surface Plasmon Resonance (SPR) and Size Exclusion Chromatography coupled to Multi Angle Light Scattering (SEC-MALS) confirmed that $MxiA_C$ forms concentration-dependent oligomers in solution (Supplementary figure 5b,d). However, SPR and SEC-MALS analyses of $MxiA_C$M5 revealed that in solution this variant was unable to associate productively under conditions identical to those used to assay the WT protein (Supplementary figure 5c,e). Moreover, purification of WT and M5 full-length MxiA-His variants in a *mxiA*$^-$ *S. flexneri* background also demonstrated that the WT protein can be isolated in an SDS-resistant oligomeric state (Supplementary figure 5h) but the M5 variant cannot.

We then sought to assay the effects of MxiA ring-disrupting mutations *in vivo* by complementing a *mxiA*$^-$ strain with either WT or mutant forms of the full length protein. As previously reported[21], the *mxiA*$^-$ strain is secretion incompetent but complementation with the WT MxiA restores secretion (Fig. 2b). Complementation with the M5 mutant, several triple and quadruple mutants, or the R545A mutant failed to restore secretion (Fig. 2b). Therefore, mutation of residues predicted on the basis of the crystal structure to disrupt ring formation, leads to *in vivo* secretion deficiencies, supporting the hypothesis that assembly of this MxiA ring is important for biological activity.

Alteration of the MxiA inner pore lining affects secretion

To further probe function, we constructed additional mutations designed to probe the external and internal faces of the ring without disrupting assembly. Earlier work on the MxiA homologue FlhA suggested a role for SD2 (now seen to be arrayed on the external surface of the ring) in selection of substrates for secretion[15]. We therefore tested *in vitro* and *in vivo* the effect of deletion of SD2 and, for comparison, mutations of solvent exposed residues on the inner surface of the ring (Fig. 3a). None of these mutations affected the ability of MxiA to self-associate *in vitro* (Supplementary figure 5f, g). Surprisingly, loss of SD2 in its entirety, despite dramatically altering the external surface of the ring, did not abolish secretion, although it did lead to a reduction in secretion of IpaC (the “translocon” component implicated in insertion of the pore in the host cell membrane) (Fig. 3b, c), with a concomitant loss of invasion capability (Fig. 3d). The single mutation K562A also perturbed the relative amounts of the secreted proteins (Fig 3b, c). By contrast, mutations of clusters of exposed residues on the inner surface of the ring (K519A R523A K562A) considerably reduced or abolished secretion (Fig. 3b). This implies that the nature of the pore is crucial for secretion and suggests that passage of secretion substrates through the center of the MxiA ring is a crucial early step in the secretory pathway.

The ring is conserved in all T3SS

Homo-nonameric symmetry is rare[30] and such an assembly has not previously been proposed for the FlhA family. Mapping amino acid conservation onto the monomer (Fig. 4, Supplementary figure 6) reveals that the oligomerizing surfaces are the most highly conserved regions of the structure amongst both flagellar and non-flagellar homologues. It is also of note that the crystal packing seen in the *Salmonella enterica* and *Bacillus subtilis* FlhA structures[15,18], both from flagellar T3SSs, depend on very similar subunit interactions (Fig. 4). This conservation of residues in the interface and independent observation of conserved subunit interactions across both flagellar and non-flagellar FlhA family members suggests that they will all assemble into nonameric rings *in vivo*. We therefore endeavored to investigate the cross-species conservation of the MxiA nonamer *in vivo*.

Location of the MxiA ring in vivo

FlhA family members have been shown to associate with the T3SS in fluorescence studies[7,9] and have been co-purified with T3SSs using gentle extraction methods[8] or in pull-down experiments (Supplementary Table 2). However, the supramolecular architecture and precise location of the FlhA with respect to the T3SS has been ambiguous due to the lack of density in the cytoplasmic regions of current EM reconstructions[28,29,31]. To date, the only *in vivo* imaging of T3SS is from flagellar systems since the additional components required for torque generation and greater size of the flagellum render these tractable to *in situ* electron cryo-tomography methods. Imaging of flagellar T3SS from a variety of bacterial species revealed a toroidal density at a consistent distance below the cytoplasmic membrane[32,33], that was proposed to contain the cytoplasmic domains of FlhA and FlhB. As the dimensions of the torus perfectly match those of the $MxiA_C$ ring (Fig. 5a), we sought to investigate whether the torus represents an *in vivo* visualization of FlhA as a nonameric ring. Since deletion of the MxiA or FlhA cytoplasmic domains abolishes secretion and hence assembly of the outer-membrane and extracellular part of the apparatus (increasing the difficulties of imaging the assembly) we have worked in *Campylobacter jejuni* where the flagellar T3SS localizes to a cellular pole and can therefore be located even in the absence of the outer membrane components and flagellum. Electron cryo-tomography produced macromolecular-resolution (2-6 nm) structures of the wild-type flagellar T3SS and the apparatus with cytoplasmic domain truncations of FlhA (*ΔflhAc*) or FlhB (*ΔflhBc*) (Fig 5b). As predicted both the *ΔflhAc* and *ΔflhBc* reconstructions lack all components beyond the inner membrane. Comparing the WT, *ΔflhAc* and *ΔflhBc* strains revealed that, although the cytoplasmic structures were largely conserved, the toroidal density previously inferred to be a FlhA- FlhB complex[32,33] was absent in the *ΔflhAc* strain but present in both the WT and *ΔflhBc* strains. In combination with the match between the size and shape of the torus and the $MxiA_C$ ring, these mutant tomograms strongly support interpretation of this torus as an $FlhA_C$ ring. The position of this ring ~ 60 Å below the inner membrane is entirely compatible with the length of the linker (45 residues) between the end of the trans-membrane helices and the start of $FlhA_C$.

Importantly, presence of a density previously ascribed to the ATPase (FliI)[32] did not change with removal of the $FlhA_C$ ring or $FlhB_C$, while removal of the ATPase did not affect the density of the torus[32]. This is consistent with the observation that the ATPase complex and the FlhA homologues associate with the T3SS independently of one another[7,34].

It is well known that the T3SS ATPase, a homo-hexameric enzyme with homology to the α/β-subunits of the F_1 ATP synthase, associates with both a central stalk, FliJ (a homologue of the F_1 γ-subunit[35]) and a peripheral stator, FliH (a homologue of the F_1 stator[36]). Our collection of tomograms[32] reveal that the distance between the FlhA torus and the ATPase density is consistent between flagellar T3SS from different species, in agreement with the

observation that the central stalk protein is relatively invariant in length and of the correct dimensions to bridge the gap. Because the T3SS ATPase is also anchored to the "C-ring", a cytoplasmic ring structure that varies in diameter across species, by its stator protein[34], we investigated the length of the stator protein in different flagellar T3SS and discovered that the distance from the ATPase to the C-ring is linearly proportional to the length of the stator (Fig.5c). The increase in size of the C-ring (increase in radius of ~1.3 Å per residue of the stator protein) is consistent with the stator adopting an extended helical conformation like that of the F_1-ATPase stator proteins.

Taken together, these data allow us to build a structural model for the major components of the T3SS export apparatus (Fig. 5d). A ring made of the FlhA family member forms the export gate of T3SSs, with the 72 predicted transmembrane helices forming the pore in the inner membrane in conjunction with the other members of the export apparatus. The large cytoplasmic ring is a key component of the apparatus through which substrates for secretion must pass thereby controlling access to the secretion pore. The cytoplasmic ATPase complex then docks underneath the FlhA nonamer via interactions with the C-ring.

DISCUSSION

Our structure and *in vivo* work suggest that the *Shigella flexneri* export apparatus component MxiA and its homologues are biologically active as export rings, and that T3SS secretion most likely proceeds by movement of substrate through the central pore of this assembly. Tomograms of flagellar T3SS lacking the homologous cytoplasmic domain establish that this export ring assembles directly below the basal body in line with the export channel at the center of the apparatus and above the ATPase complex. Furthermore, both the export ring and the ATPase complex assemble independently of each other.

Previous work has demonstrated that the T3SS ATPase complex is structurally homologous to the well-characterised F_1F_0 ATP synthase complex[35,37,38], that secretion by the export apparatus is proton motive force driven[39-43] and that the FlhA transmembrane helices are involved in this process[44].

Using our new architecture to interpret these earlier observations allows us to propose a novel model for the way in which FlhA family members interact with the rest of the apparatus to promote secretion of substrates (Fig 6). In particular, we note that the cytoplasmic export ring pore (Fig 6a), revealed in our structure of the cytoplasmic domain, is of sufficient size to allow passage of folded or only partially unfolded substrates, in contrast to the pore in the needle or in the flagellum that requires unfolding to the level of isolated helices or extended polypeptide[3]. Work by others has implicated the ATPase complex in recruitment of substrate-chaperone complexes to the export apparatus[38,45-47] presumably aided by interactions with other export apparatus components[13] and with the external surface of the export ring in a substrate specific fashion (this work and[15,16]). Following separation of the chaperone we then speculate that the largely folded substrate is admitted to an export cage via the central pore formed by the annular arrangement of the cytoplasmic and transmembrane domains of FlhA homologues and that the proton motive force driven secretion of the substrate is mediated from this membrane proximal but relatively isolated location. Our architecture for the major export apparatus component and its positioning with respect to the relatively membrane distant ATPase complex is strongly reminiscent of the architecture of the F_1F_0 ATP synthase complex perhaps implying that there may be greater mechanistic similarities between these systems. Such similarities suggest that one possible mechanism for coupling of ATP hydrolysis at this membrane distant location to use of proton motive force in secretion is via γ-subunit mediated rotation/ induction of conformational change of the export cage. Much further work will be required

to test this model and to elucidate the role of the other export apparatus components, but we note that there is room for multiple copies of the other key export apparatus components in addition to the nine copies of the FlhA family member, suggested by our structure of the cytoplasmic domain, within the basal body. Differences in the nature of the export-ring pore and system-specific accessory proteins and chaperones will add further mechanisms for control of export. We also note that tethering of the ATPase complex to the C-ring, which is thought to rotate at least in the flagellar systems[48], also raises questions about potential additional roles for rotation in driving secretion which will need to be investigated in further studies.

Online methods

DNA manipulation, bacterial growth and protein expression conditions

Recombinant expression of $MxiA_C$ in the *E. coli* C41(DE3) strain[52] transformed with the plasmid pACYC_6His$MxiA_C$ was obtained with 16 hours induction at 21°C by 1 mM IPTG. For the expression of the export apparatus complex, the *E. coli* L56(DE3) strain was co-transformed with the plasmids pET_MxiA6His and pACYC_Spa24-29ORF, the latter being a polycistron vector, and the induction was carried on at 24°C for 16 hours with 0.1 mM IPTG. *mxiA*$^-$ *S. flexneri* strain was created inserting a double stop codon after the first methionine through homologous recombination with pKO3blue plasmid[53]. For complementation assays, *mxiA*$^-$ *S. flexneri* strain was transformed with the plasmid expressing the His-tagged full-length MxiA (pBAD_MxiA6His) in the presence of 0.02% arabinose. Mutations to validate the authenticity and the function of MxiA ring *in vitro* and *in vivo* were introduced in the appropriate plasmid by site direct mutagenesis using the XLQuickChange Kit (Agilent). Constructs were verified by DNA sequencing. Resulting plasmids were transformed into the appropriate host by electroporation or heat shock method.

E. coli strains were grown in Luria-Bertani medium (LB; Invitrogen), Terrific broth (TB; Fisher) or on LB agar. *S. flexneri* strains were propagated in LB broth and LB agar plates with 0.01% Congo Red (CR) in the presence of 100 μg ml^{-1} Ampicillin and 20 μg ml^{-1} Chloramphenicol, when required.

PCR-mediated mutagenesis was used to fuse the codon for Thr320 to the stop codon of *C. jejuni* 81-176 *flhA* in pDRH664 to generate $flhA_C$, which lacks the region of *flhA* encoding the C-terminal 391 amino acid predicted to encompass the cytoplasmic domain of FlhA[54]. The resulting plasmid, pDRH2505, was used to electroporate *C. jejuni* 81-176 *rpsL*^{Sm} *flhA::cat-rpsL* (DRH901;[54]) to replace *flhA::cat-rpsL* on the chromosome with $flhA_C$. Transformants were selected on 0.5, 1, 2, and 5 mg ml^{-1} Streptomycin and screened by colony PCR for acquisition of $flhA_C$ at the native locus on the chromosome, resulting in *C. jejuni* 81-176 *rpsL*^{Sm} $flhA_C$ (SNJ833).

Supplementary table 3 lists strains and plasmids used in this study.

Secretion and invasion assays

Secretion assays were performed according to Kenjale *et al.*[55]. Ipa proteins were identified by immunoblotting. All samples were initially normalized for bacterial density. RecA was used as loading control. *S. flexneri* invasion of HeLa cells was monitored as described elsewhere[56]. Results were expressed as percentage of intracellular bacteria in relation to the input.

Structure determination

Cells expressing $MxiA_C$ as N-terminal 6His-tagged protein were harvested and lysed by homogenization. The clarified lysate containing the soluble recombinant protein was subjected to immobilized metal affinity chromatography (IMAC) followed by size-exclusion chromatography (SEC). $MxiA_C$, purified to homogeneity, was then reductive methylated by dimethylamine borane complex (DMAB) and formaldehyde[57] and then subjected to a second SEC step. Methylated $MxiA_C$ (6 mg ml^{-1}) in 20 mM PIPES (pH 7.0), 150 mM NaCl, 5 mM KCl, 5% glycerol, 1 mM EDTA and 1 mM DTT was exclusively used for crystallization experiments. Crystallization screening used commercial sparse matrix screens (Molecular Dimensions) in vapor diffusion with 0.2 μl sitting drops. Methylated $MxiA_C$ crystallized from mother-liquor containing 0.1 M sodium-HEPES buffer (pH 7.5), 10% (w/v) PEG 8,000 and 8% ethylene glycol at 12°C. Crystals were cryo-protected using mother liquor supplemented with 25% EG.

X-ray diffraction data were collected on beamline I03 at Diamond Light Source synchrotron, indexed and integrated using Xia2[58]. SCALA and TRUNCATE from CCP4i suite[59] were used for scaling and merging of diffraction data (Table 1) and calculation of structure factor amplitudes. The initial phases were determined by molecular replacement with PHASER[59] using InvA (PDB: 2X4A) as search model. Initial phases were markedly improved by iterative cycles of solvent flattening, and three-fold noncrystallographic symmetry averaging with DM[59]. The preliminary model was built by Buccaneer and then manually completed in COOT [60]. Several rounds of structure refinement (using autoBUSTER[61]) yielded the model described in the Table 1. Structure validation was performed with MolProbity (http://molprobity.biochem.duke.edu/), resulting in Rmachandran statistics with 98.7% of residues in favored or allowed regions and no outliers and an overall MolProbity score of 1.56. Figures were prepared using the program PyMol (http://pymol.org/) and ESPript (http://espript.ibcp.fr/ESPript/ESPript/).

In vitro characterization of the multimeric assembly

Absolute molar mass and mass distribution of purified $MxiA_C$ variants were determined using SEC-MALS by injecting through a Superdex 200 10/300 GL or a Superose 6 10/300 GL column equilibrated in a TBS buffer (20 mM Tris-HCl pH8.0 and 150 mM NaCl) followed in-line by a Dawn Heleos-II light scattering detector (Wyatt Technologies) and an Optilab-Rex refractive index monitor (Wyatt Technologies). Molecular mass calculations were performed using ASTRA 5.3.4.14 (Wyatt Technologies) assuming a dn/dc value of 0.186 ml g^{-1}.

$MxiA_C$ was chemically cross-linked using dimethyl 3,3′-dithiobispropionimidate*2HCl (DTBP) (Thermo Fisher Scientific). Briefly, $MxiA_C$ was cross-linked with 10 fold molar excess of DTBP at room temperature for 1 hour and then the reaction was quenched adding an excess of TRIS-HCl pH 6.8. Samples treated with and without DTBP were loaded on an 8% SDS-PAGE and the subjected to Western Blot using an anti-His HRP-conjugated (Qiagen) for the immunodetection.

Mass spectrometry analyses were performed at the Central Proteomic Facility of Dunn School of Pathology. Automated data analyses were performed using Mascot as search engine in the local Proteomic Data analysis Pipeline.

Recombinant EA complex

Cells co-expressing the full length MxiA (1-686), fused to a Myc-His C terminal tag, with Spa24, Spa9 and Spa29 were harvested and lysed by homogenization. The clarified lysate was centrifuged at 150.000*g* for 1h at 4°C in order to pellet the membrane fraction, which

was then solubilized in PBS supplemented with 1% DDM at ~15 mg ml^{-1} for 1 hour at 4°C. After centrifugation at 150.000*g* for 1h, the detergent-solubilized complex was purified by IMAC and then dialyzed overnight into PBS with 0.03% DDM.

Native PAGE was performed using Biorad 4-20% Mini-PROTEAN TGX precast gels according to manufacturer instructions at 150V for 100 minutes. The gel was then stained for a few minutes in 0.1% Ponceau S solution and the band of interest cropped with a sterile blade. The band was then incubated for 30 min in 2x Laemmli loading buffer supplemented with 50 mM DTT, subsequently layered onto a 15% SDS acrylamide running gel and sealed with 2.5 ml of stacking gel mixture. The SDS-PAGE was performed for 120 minutes at 120V and then the gel was Coomassie stained. An equivalent gel was blotted onto a PVDF membrane and the immunodetection was performed using the Qiagen Penta-His HRP Conjugate Kit. The identity of the MxiA band was also confirmed by trypsin digest-mass spectrometry analysis (data not shown).

Absolute molar mass was determined using MALS in batch mode by injecting 120μl of sample at 0.6 mg ml^{-1} through a system equilibrated in PBS with 0.03% DDM and coupled to multi-angle light scattering and refractive index detectors (Wyatt Technology). Data analyses were carried out as before.

Electron cryo-tomography

C. jejuni 81-176 strain SNJ833 was grown and imaged as previously described for *C. jejuni 81*-176 Sm^R *ΔastA ΔfliF*[32] except reconstruction using an implementation of the SIRT algorithm[62] after low-pass filtering to 5.5 nm resolution, co-incident with the first zero of the CTF at -15 μm defocus. Resultant tomograms had a pixel size of 1.56 nm. A number of 49 motor assembly intermediates were hand picked, then computationally aligned and averaged, without subsequent symmetrization, using the PEET software suite[63].

Supplementary Material

Refer to Web version on PubMed Central for supplementary material.

Acknowledgments

We thank N. Strynadka for access to InvA coordinates ahead of publication, P. Sansonetti for kindly providing the polyclonal antibodies against Ipa proteins and I. Lasa for the pKO3blue plasmid. L. De Colibus, C. King and members of the Lea group are thanked for general assistance. The staff of the protein crystallography beamlines at the European Synchrotron Radiation Source, Grenoble (France) and DIAMOND facility, Didcot (UK) are thanked for assistance in data collection and S. K. Mazmanian for use of the microaerobic chamber.

P.A. is funded by grant 083599/Z/07/Z and J.E.D. by grant WT083599MA both from the Wellcome Trust to S.M.L., S.J. by grant G0900888 from the Medical Research Council (UK) to S.M.L. and P.R. are funded by the Oxford Martin School Vaccine Design Institute of which S.M.L. is co-director. M.V.I. is funded by FP7 Marie Curie EIMID-IAPP-217768 grant. M.B. and G.J.J. were supported by the Howard Hughes Medical Institute.

References

1. Cornelis GR. The type III secretion injectisome, a complex nanomachine for intracellular ‘toxin’ delivery. Biological chemistry. 2010; 391:745–51. [PubMed: 20482311]
2. Patel JC, Galan JE. Manipulation of the host actin cytoskeleton by Salmonella--all in the name of entry. Current opinion in microbiology. 2005; 8:10–5. [PubMed: 15694851]
3. Blocker AJ, et al. What’s the point of the type III secretion system needle? Proceedings of the National Academy of Sciences of the United States of America. 2008; 105:6507–13. [PubMed: 18458349]

4. Erhardt M, Namba K, Hughes KT. Bacterial nanomachines: the flagellum and type III injectisome. Cold Spring Harbor perspectives in biology. 2010; 2:a000299. [PubMed: 20926516]
5. Marlovits TC, Stebbins CE. Type III secretion systems shape up as they ship out. Current opinion in microbiology. 2010; 13:47–52. [PubMed: 20015680]
6. Deane JE, Abrusci P, Johnson S, Lea SM. Timing is everything:the regulation of type III secretion. Cellular and molecular life sciences : CMLS. 2010; 67:1065–75. [PubMed: 20043184]
7. Diepold A, Wiesand U, Cornelis GR. The assembly of the export apparatus (YscR,S,T,U,V) of the Yersinia type III secretion apparatus occurs independently of other structural components and involves the formation of an YscV oligomer. Molecular microbiology. 2011
8. Wagner S, et al. Organization and coordinated assembly of the type III secretion export apparatus. Proceedings of the National Academy of Sciences of the United States of America. 2010; 107:17745–50. [PubMed: 20876096]
9. Li H, Sourjik V. Assembly and stability of flagellar motor in Escherichia coli. Molecular microbiology. 2011; 80:886–99. [PubMed: 21244534]
10. Minamino T, Imada K, Namba K. Mechanisms of type III protein export for bacterial flagellar assembly. Molecular bioSystems. 2008; 4:1105–15. [PubMed: 18931786]
11. Minamino T, Imada K, Namba K. Molecular motors of the bacterial flagella. Current opinion in structural biology. 2008; 18:693–701. [PubMed: 18848888]
12. Diepold A, et al. Deciphering the assembly of the Yersinia type III secretion injectisome. The EMBO journal. 2010; 29:1928–40. [PubMed: 20453832]
13. Zhu K, Gonzalez-Pedrajo B, Macnab RM. Interactions among membrane and soluble components of the flagellar export apparatus of Salmonella. Biochemistry. 2002; 41:9516–24. [PubMed: 12135374]
14. McMurry JL, Van Arnam JS, Kihara M, Macnab RM. Analysis of the cytoplasmic domains of Salmonella FlhA and interactions with components of the flagellar export machinery. Journal of bacteriology. 2004; 186:7586–92. [PubMed: 15516571]
15. Bange G, et al. FlhA provides the adaptor for coordinated delivery of late flagella building blocks to the type III secretion system. Proceedings of the National Academy of Sciences of the United States of America. 2010; 107:11295–300. [PubMed: 20534509]
16. Minamino T, et al. Interaction of a bacterial flagellar chaperone FlgN with FlhA is required for efficient export of its cognate substrates. Molecular microbiology. 2012; 83:775–788. [PubMed: 22233518]
17. Worrall LJ, Vuckovic M, Strynadka NC. Crystal structure of the C-terminal domain of the Salmonella type III secretion system export apparatus protein InvA. Protein science : a publication of the Protein Society. 2010; 19:1091–6. [PubMed: 20306492]
18. Saijo-Hamano Y, et al. Structure of the cytoplasmic domain of FlhA and implication for flagellar type III protein export. Molecular microbiology. 2010; 76:260–8. [PubMed: 20199603]
19. Moore SA, Jia Y. Structure of the cytoplasmic domain of the flagellar secretion apparatus component FlhA from Helicobacter pylori. The Journal of biological chemistry. 2010; 285:21060–9. [PubMed: 20442410]
20. Lilic M, Quezada CM, Stebbins CE. A conserved domain in type III secretion links the cytoplasmic domain of InvA to elements of the basal body. Acta crystallographica Section D, Biological crystallography. 2010; 66:709–13.
21. Andrews GP, Maurelli AT. mxiA of Shigella flexneri 2a, which facilitates export of invasion plasmid antigens, encodes a homolog of the low-calcium-response protein, LcrD, of Yersinia pestis. Infection and immunity. 1992; 60:3287–95. [PubMed: 1639496]
22. Ashida H, et al. Shigella deploy multiple countermeasures against host innate immune responses. Current opinion in microbiology. 2011; 14:16–23. [PubMed: 20934372]
23. Spreter T, et al. A conserved structural motif mediates formation of the periplasmic rings in the type III secretion system. Nature structural & molecular biology. 2009; 16:468–76.
24. Worrall LJ, Lameignere E, Strynadka NC. Structural overview of the bacterial injectisome. Current opinion in microbiology. 2011; 14:3–8. [PubMed: 21112241]
25. Yip CK, et al. Structural characterization of the molecular platform for type III secretion system assembly. Nature. 2005; 435:702–7. [PubMed: 15931226]

26. Sanowar S, et al. Interactions of the Transmembrane Polymeric Rings of the Salmonella enterica Serovar Typhimurium Type III Secretion System. mBio. 2010; 1
27. Lee LK, Ginsburg MA, Crovace C, Donohoe M, Stock D. Structure of the torque ring of the flagellar motor and the molecular basis for rotational switching. Nature. 2010; 466:996–1000. [PubMed: 20676082]
28. Schraidt O, Marlovits TC. Three-dimensional model of Salmonella's needle complex at subnanometer resolution. Science. 2011; 331:1192–5. [PubMed: 21385715]
29. Hodgkinson JL, et al. Three-dimensional reconstruction of the Shigella T3SS transmembrane regions reveals 12-fold symmetry and novel features throughout. Nature structural & molecular biology. 2009; 16:477–85.
30. Goodsell DS, Olson AJ. Structural symmetry and protein function. Annual review of biophysics and biomolecular structure. 2000; 29:105–53.
31. Thomas DR, Francis NR, Xu C, DeRosier DJ. The three-dimensional structure of the flagellar rotor from a clockwise-locked mutant of Salmonella enterica serovar Typhimurium. Journal of bacteriology. 2006; 188:7039–48. [PubMed: 17015643]
32. Chen S, et al. Structural diversity of bacterial flagellar motors. The EMBO journal. 2011; 30:2972–81. [PubMed: 21673657]
33. Liu J, et al. Intact flagellar motor of Borrelia burgdorferi revealed by cryo-electron tomography: evidence for stator ring curvature and rotor/C-ring assembly flexion. Journal of bacteriology. 2009; 191:5026–36. [PubMed: 19429612]
34. Minamino T, et al. Roles of the extreme N-terminal region of FliH for efficient localization of the FliH-FliI complex to the bacterial flagellar type III export apparatus. Molecular microbiology. 2009; 74:1471–83. [PubMed: 19889085]
35. Ibuki T, et al. Common architecture of the flagellar type III protein export apparatus and F- and V-type ATPases. Nature structural & molecular biology. 2011; 18:277–82.
36. Pallen MJ, Bailey CM, Beatson SA. Evolutionary links between FliH/YscL-like proteins from bacterial type III secretion systems and second-stalk components of the FoF1 and vacuolar ATPases. Protein science : a publication of the Protein Society. 2006; 15:935–41. [PubMed: 16522800]
37. Imada K, Minamino T, Tahara A, Namba K. Structural similarity between the flagellar type III ATPase FliI and F1-ATPase subunits. Proceedings of the National Academy of Sciences of the United States of America. 2007; 104:485–90. [PubMed: 17202259]
38. Zarivach R, Vuckovic M, Deng W, Finlay BB, Strynadka NC. Structural analysis of a prototypical ATPase from the type III secretion system. Nature structural & molecular biology. 2007; 14:131–7.
39. Minamino T, Morimoto YV, Hara N, Namba K. An energy transduction mechanism used in bacterial flagellar type III protein export. Nature communications. 2011; 2:475.
40. Paul K, Erhardt M, Hirano T, Blair DF, Hughes KT. Energy source of flagellar type III secretion. Nature. 2008; 451:489–92. [PubMed: 18216859]
41. Minamino T, Namba K. Distinct roles of the FliI ATPase and proton motive force in bacterial flagellar protein export. Nature. 2008; 451:485–8. [PubMed: 18216858]
42. Wilharm G, et al. Yersinia enterocolitica type III secretion depends on the proton motive force but not on the flagellar motor components MotA and MotB. Infection and immunity. 2004; 72:4004–9. [PubMed: 15213145]
43. Galperin M, Dibrov PA, Glagolev AN. delta mu H+ is required for flagellar growth in Escherichia coli. FEBS letters. 1982; 143:319–22. [PubMed: 6811323]
44. Hara N, Namba K, Minamino T. Genetic Characterization of Conserved Charged Residues in the Bacterial Flagellar Type III Export Protein FlhA. PloS one. 2011; 6:e22417. [PubMed: 21811603]
45. Minamino T, Kinoshita M, Imada K, Namba K. Interaction between FliI ATPase and a flagellar chaperone FliT during bacterial flagellar protein export. Molecular microbiology. 2012; 83:168–78. [PubMed: 22111876]
46. Akeda Y, Galan JE. Chaperone release and unfolding of substrates in type III secretion. Nature. 2005; 437:911–5. [PubMed: 16208377]

47. Thomas J, Stafford GP, Hughes C. Docking of cytosolic chaperone-substrate complexes at the membrane ATPase during flagellar type III protein export. Proceedings of the National Academy of Sciences of the United States of America. 2004; 101:3945–50. [PubMed: 15001708]
48. Berg HC. The rotary motor of bacterial flagella. Annual review of biochemistry. 2003; 72:19–54.
49. Murphy GE, Leadbetter JR, Jensen GJ. In situ structure of the complete Treponema primitia flagellar motor. Nature. 2006; 442:1062–4. [PubMed: 16885937]
50. Blocker A, et al. Structure and composition of the Shigella flexneri “needle complex”, a part of its type III secreton. Molecular microbiology. 2001; 39:652–63. [PubMed: 11169106]
51. Wolf S, Freier E, Potschies M, Hofmann E, Gerwert K. Directional proton transfer in membrane proteins achieved through protonated protein-bound water molecules: a proton diode. Angewandte Chemie. 2010; 49:6889–93. [PubMed: 20680951]
52. Miroux B, Walker JE. Over-production of proteins in Escherichia coli: mutant hosts that allow synthesis of some membrane proteins and globular proteins at high levels. Journal of molecular biology. 1996; 260:289–98. [PubMed: 8757792]
53. Solano C, et al. Genetic reductionist approach for dissecting individual roles of GGDEF proteins within the c-di-GMP signaling network in Salmonella. Proceedings of the National Academy of Sciences of the United States of America. 2009; 106:7997–8002. [PubMed: 19416883]
54. Hendrixson DR, DiRita VJ. Transcription of sigma54-dependent but not sigma28-dependent flagellar genes in Campylobacter jejuni is associated with formation of the flagellar secretory apparatus. Molecular microbiology. 2003; 50:687–702. [PubMed: 14617189]
55. Kenjale R, et al. The needle component of the type III secreton of Shigella regulates the activity of the secretion apparatus. The Journal of biological chemistry. 2005; 280:42929–37. [PubMed: 16227202]
56. Marteyn B, et al. Modulation of Shigella virulence in response to available oxygen in vivo. Nature. 2010; 465:355–8. [PubMed: 20436458]
57. Rayment I. Reductive alkylation of lysine residues to alter crystallization properties of proteins. Methods in enzymology. 1997; 276:171–9. [PubMed: 9048376]
58. Winter G. xia2: an expert system for macromolecular crystallography data reduction. Journal of Applied Crystallography. 2010; 43:186–190.
59. The CCP4 suite: programs for protein crystallography. Acta crystallographica Section D, Biological crystallography. 1994; 50:760–3.
60. Emsley P, Lohkamp B, Scott WG, Cowtan K. Features and development of Coot. Acta crystallographica Section D, Biological crystallography. 2010; 66:486–501.
61. Blanc E, et al. Refinement of severely incomplete structures with maximum likelihood in BUSTER-TNT. Acta crystallographica Section D, Biological crystallography. 2004; 60:2210–21.
62. Agulleiro JI, Fernandez JJ. Fast tomographic reconstruction on multicore computers. Bioinformatics. 2011; 27:582–3. [PubMed: 21172911]
63. Nicastro D, et al. The molecular architecture of axonemes revealed by cryoelectron tomography. Science. 2006; 313:944–8. [PubMed: 16917055]

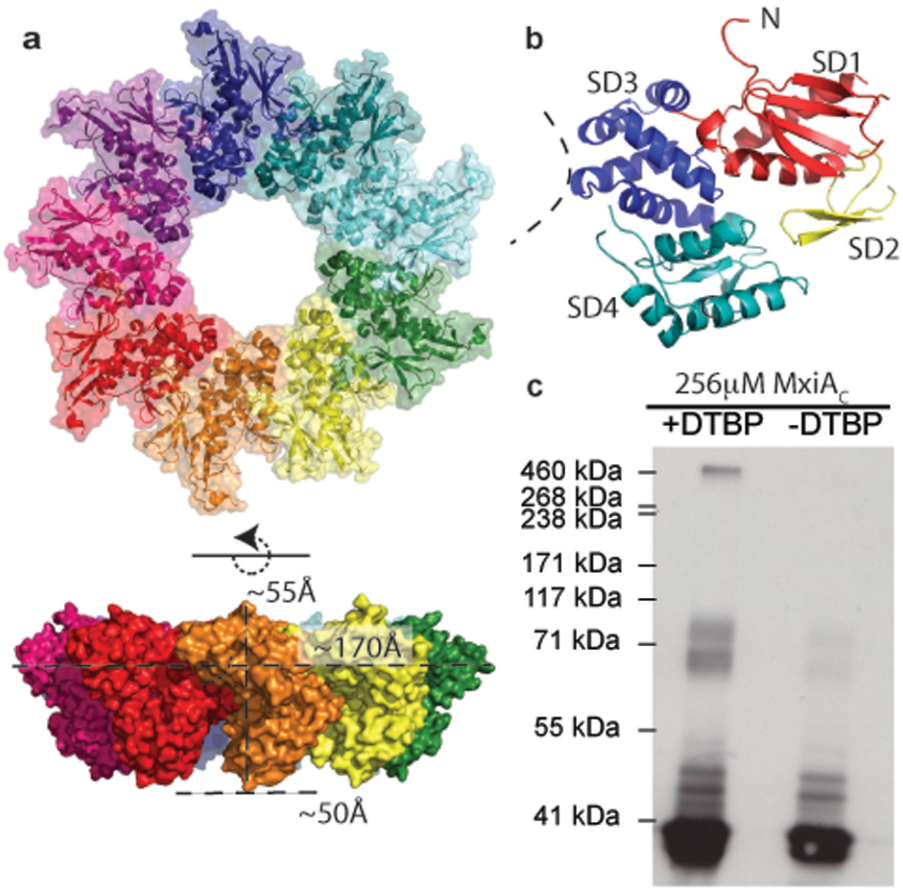

Figure 1. MxiA$_C$ crystallize as a nonameric ring

(a) Representation of MxiA$_C$ ring structure as surface and cartoon, top and lateral views colored by chain.

(b) Boundaries of MxiA$_C$ subdomains: SD1 (residues: 356-428, 478-493) red; SD2 (residues: 429-477) yellow; SD3 (residues: 494-583) blue; SD4 (residues: 584-686) cyan. The inner ring surface is indicated as a dashed line.

(c) Immunoblotting of MxiA$_C$ cross-linked by DTBP.

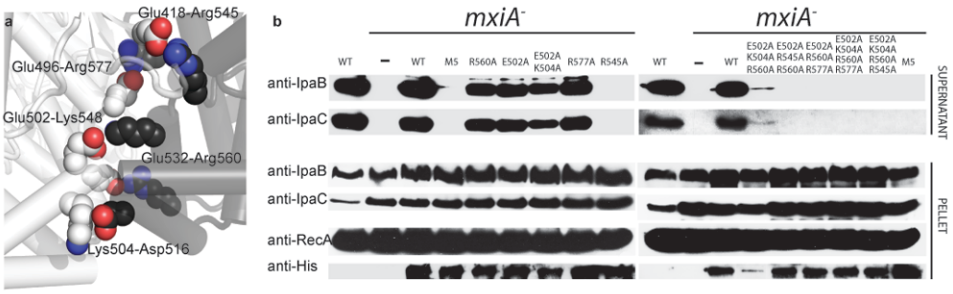

Figure 2. *In vitro* and *in vivo* analysis of the MxiA ring

(a) Close-up of interface between monomers highlights intermolecular salt bridging residues with their side chains represented as sphere.

(b) Immunodetection by western blots of IpaBC in bacterial supernatants (upper panel) and pellet (lower panel) for complemented *mxiA*⁻ *Shigella* strains upon CR stimulation. Complementation with M5, R545A, several triple and quadruple mutations fail to restore secretion, despite the fact that all complemented strains express secretion substrates at normal level (lower panel) and the expression of all MxiA variants is comparable to the WT level with the only exception of the mutant E502A-K504A-R560A (anti-His strip, pellet panel).

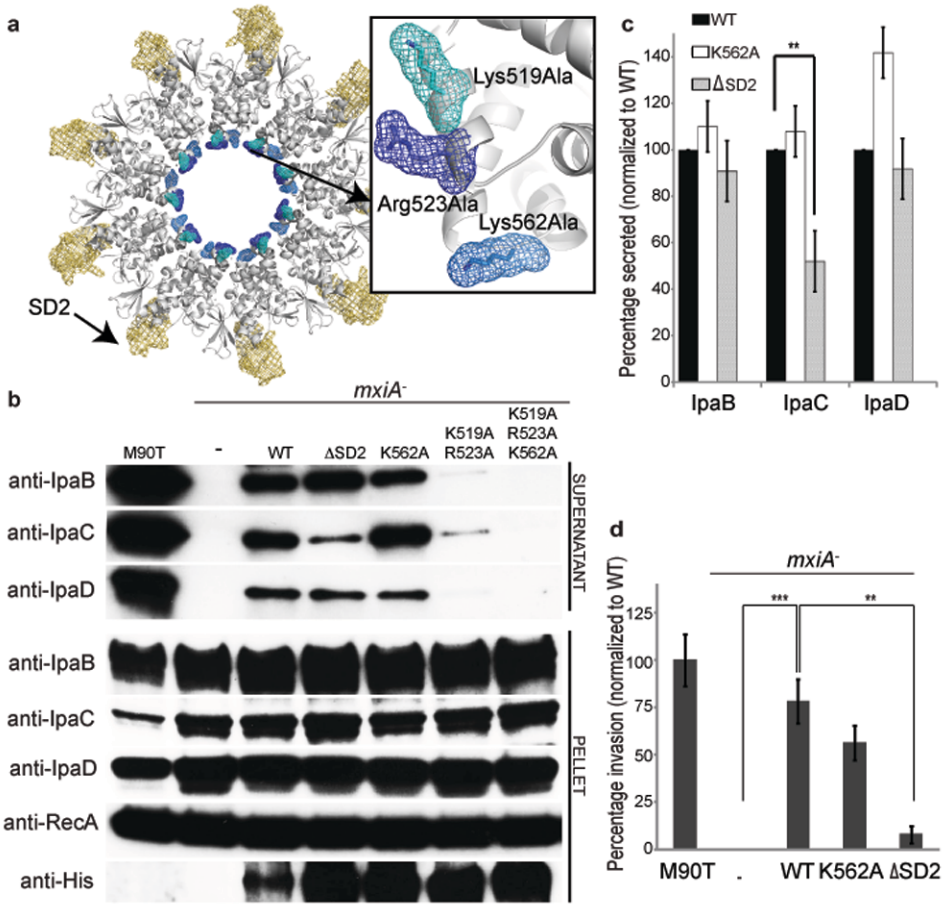

Figure 3. Altering the inner and outer surfaces of the MxiA ring

(a) Surface of the outer SD2 is represented in yellow mesh surface whilst K519, R523 and K562 are represented in shades of blue. Close-up of the inner surface of the ring on the right.

(b) Detection of IpaB, C and D in bacterial supernatants (upper panel) and pellet (lower panel) by immunoblotting upon Congo Red stimulation for complemented *mxiA*$^{-}$ *Shigella* strains. Double and triple mutants fail to restore secretion although expression of these variants in the bacterial pellet is comparable to the WT level (His strip, pellet panel).

(c) Histogram of the percentage of IpaB, C and D secreted as fraction of the WT. Data are calculated from three independent experiments and the standard error of the mean is represented as error bars. Significant differences are detected using a one way ANOVA and pairwise comparisons made using the Holm-Sidak test. Differences are considered statistically significant for $P<0.05$; (**) indicates $P<0.005$.

(d) Invasion assay performed on HeLa epithelial cells. The deletion of the SD2 greatly decreases the invasion efficiency, in accordance with the reduction of the IpaC secretion. K562A does not affect the invasion ability. Results are normalized to M90T wild type strain (100%). Data represent the means of six independent experiments performed in triplicate (error bars represent the standard deviation). Significant differences are detected using a Student's t-test. Differences are considered statistically significant for $P<0.05$; (**) means $P<0.01$; (***) means $P<0.001$.

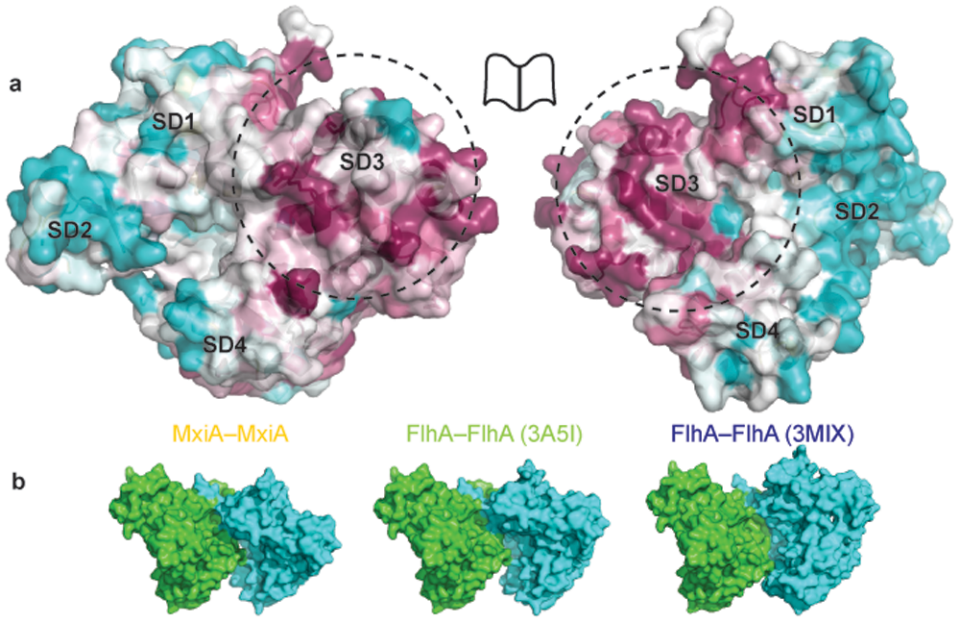

Figure 4. MxiA$_C$ surface conservation

(a) Surface residues are colored in accordance with evolutionary conservation (high=purple, low=cyan) among amino acid sequences from 30 members of the FlhA family. These figures were prepared using ConSurf (http://consurf.tau.ac.il/). The black line marks the footprint of the interface between monomers in MxiA$_C$, *Salmonella* FlhA$_C$ (3A5I) and *Bacillus* FlhA$_C$ (3MIX) crystal structures.

(b) MxiA$_C$ monomers (left) are shown reoriented to match the molecular packing found in the *Salmonella* FhlA$_C$ (middle) and *Bacillus* FlhA$_C$ (right) crystal structures to highlight that both flagellar MxiA counterparts associate with the same interface as MxiA$_C$.

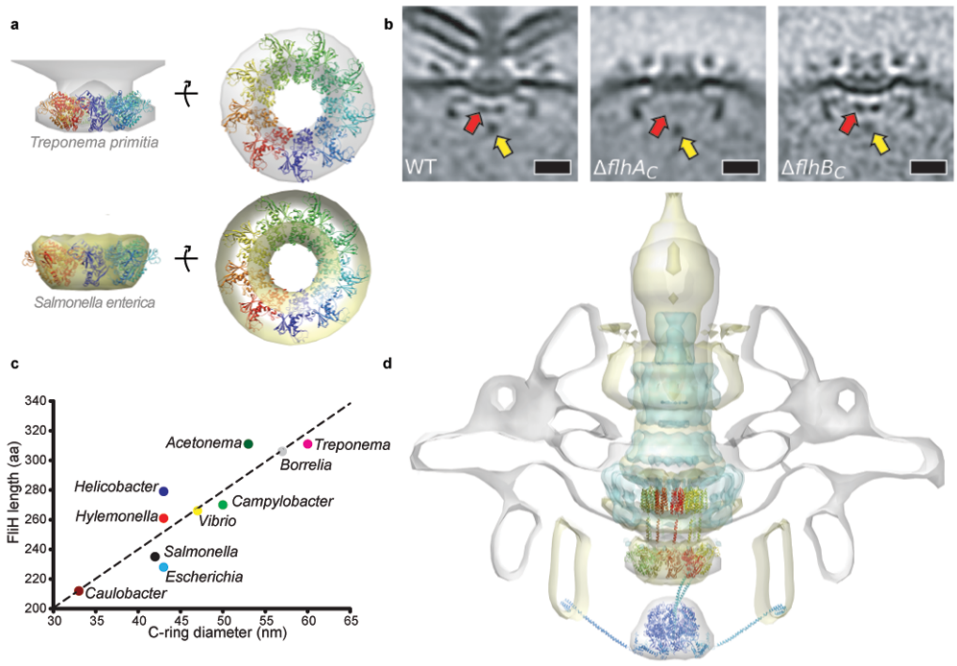

Figure 5. Model for MxiA architecture within the T3SS

(a) The dimensions of the nonameric MxiA ring fit the inner-membrane proximal density observed in *in situ* cryotomograms of flagellar T3SS from *Treponema primitia*[49] and *Samonella enterica* [32]. Both models are represented as side and top view.

(b) *in situ* subtomogram averages identifying the location of $MxiA_C$ homolog in the *Campylobacter jejuni* flagellar T3SS: **(left)** wild-type, **(middle)** truncation of the cytoplasmic domain of MxiA homolog FlhA, **(right)** truncation of cytoplasmic domain of Spa40 homolog FlhB. Red arrow indicates the toroidal density. Yellow arrow indicates the density of the ATPase. 20 nm scale bar is shown.

(c) Correlation between stator protein length and C-ring diameter in selected cryotomograms of flagellar motors[32,49]. R^2=0.8115.

(d) A model for the intact MxiA (including linker and transmembrane domains) is positioned in overlaid cryotomograms (*Treponema*-grey, *Salmonella*-yellow). The EM reconstruction of the *Shigella flexneri* T3SS[50] (cyan) is also overlaid for comparison. The MxiA transmembrane ring is modeled using bacterorhodopsin (PDB_ID:2WJK[51]) and the linker between the cytoplasmic and transmembrane rings is modeled as an arbitrary 36-amino acid helix. This model is completed with the hexameric FliI (PDB_ID:2DPY[37]) located as previously determined[32], FliJ (PDB_ID:3AJW[35]) and a model of FliH.

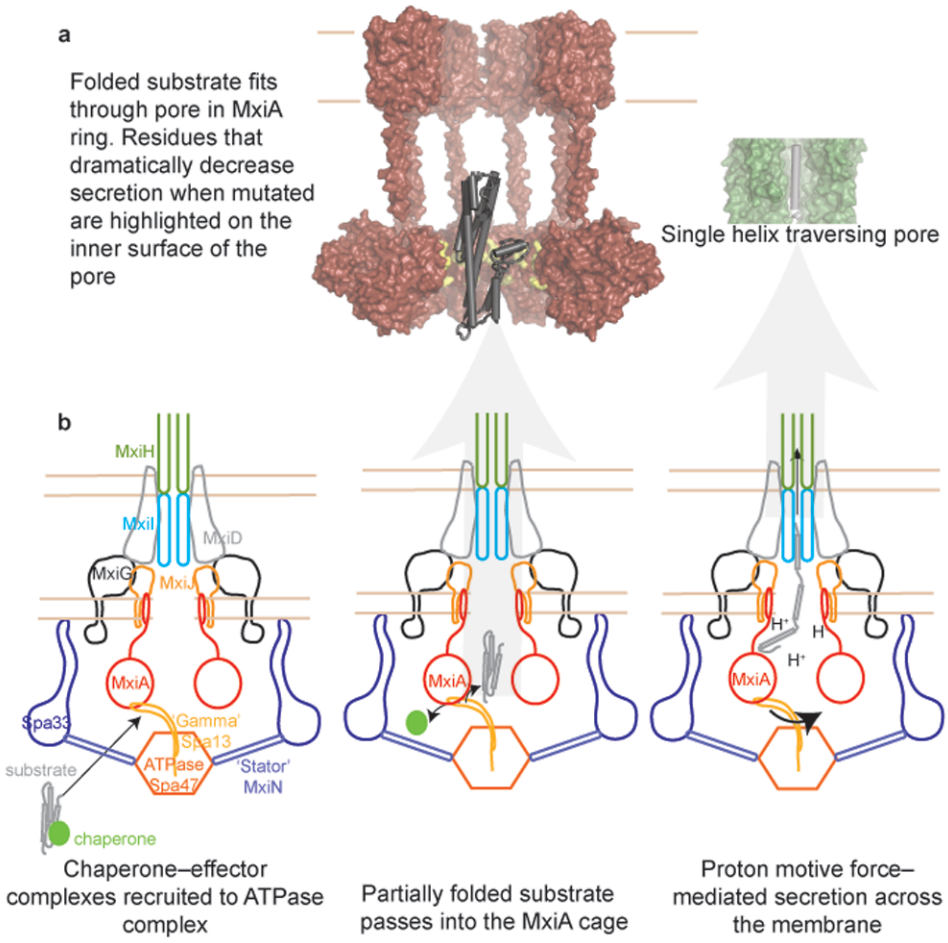

Figure 6. Mechanistic model of T3SS secretion

(a) On the left panel, slab view of the exporting cage loaded with substrate (IpaD, PDB ID: 2J0O). MxiA model is represented as dark red surface with residues crucial for the function of the export-ring pore, highlighted in yellow. IpaD structure is in dark gray. On the right panel, slab view of the needle with a traversing helix.

(b) 3-view cartoon of key steps in T3SS secretion: 1) chaperone-effector complex is recruited to the ATPase level; 2) the ATPase complex ‘strips’ the chaperone from the exporting substrate and allowing the partially folded substrate to enter the exporting cage; 3) proton motive force mediated secretion of the unfolded substrate through the hollow needle. This simplified diagram does not show the other export apparatus components (Spa24, Spa9, Spa29 and Spa40), although they act to nucleate the MxiA assembly in the nascent export apparatus or MxiK which is thought to aid assembly of Spa33. See text and Supplementary Table 1 for details.

Table 1

Data collection and refinement statistics (molecular replacement)

Data collection	
Space group	$P6_3$
Cell dimensions	
a, *b*, *c* (Å)	160.61,160.61,100.49
α, β, γ (°)	90, 90, 120
Resolution (Å)	81.5-3.15(3.24-3.15)
R_{sym} or R_{merge}	7.7 (53.6)
$I / \sigma I$	11.5 (2.0)
Completeness (%)	94.3 (96.0)
Redundancy	2.6(2.6)
Refinement	
Resolution (Å)	36-3.15 (3.29-3.15)
No. reflections	23965 (1785)
R_{work} / R_{free}	23.1% /25.1%
No. atoms	
Protein	699
Ligand/ion	492
Water	16
B-factors	
Protein	76.791
Ligand/ion	67.2
Water	30.982
R.m.s. deviations	
Bond lengths (Å)	0.008
Bond angles (°)	0.88

*Values in parentheses are for highest-resolution shell.